Experimental and Analytical Studies of Iodine Mass Transfer from Xenon-Iodine Mixed Gas Bubble to Liquid Sodium Pool

S. Miyahara, N. Sagawa and K. Shimoyama
O-arai Engineering Center
Power Reactor and Nuclear Fuel Development Corporation
O-arai, Ibaraki, 311-13 Japan

Abstract

In the fuel pin failure accident of a liquid metal fast reactor, volatile fission products play an important role in the assessment of radiological consequences. Especially the radioisotopes of elemental iodine are important because of their high volatility and of the low permissible dose to human thyroid. The released iodines are known to be retained in the coolant sodium as sodium iodide due to the chemical affinity between alkali metals and halogens. However, the xenon and krypton released with iodines into the sodium pool as bubbles may influence the reaction rate of iodine with sodium during the bubble rising. So far, the only few experimental results have been available concerning the decontamination factor (DF: the ratio of the initial iodine mass in the mixed gas bubble to the released mass into the cover gas) of iodine in this phenomenon. Therefore, experimental and analytical studies were carried out to study the mass transfer of iodine from a xenon-iodine mixed gas bubble to the liquid sodium pool.

In the experiments, the bubble was generated in the sodium pool by cracking a quartz ball which contains the xenon-iodine mixed gas and then, the mixed gas released into the argon cover gas was collected to determine the transferred iodine mass into the pool. A rising velocity of the bubble was measured by Chen-type void sensors arranged vertically in the pool.

From the measured rising velocity and another observation of bubble behavior in simulated water experiments, it is found that the generated bubble breaks up into several smaller bubbles of spherical cap type during the rising period.

Transferred iodine mass per unit initial bubble volume from the bubble to the sodium pool shows increases with increasing time and the initial iodine concentration. A mass transfer rate obtained by differentiating the transferred iodine mass with respect to the time indicates a rapid decrease just after the bubble generation and a slow decrease for the successive period. Measured DFs are described as a function of the time and the iodine concentration.

To clarify the process of the iodine mass transfer in a xenon-iodine mixed gas bubble rising through the liquid sodium pool, the mass transfer is analyzed on the basis of a diffusion model applied to the first short stage just after the bubble generation and a convection model applied to the successive stage. In the diffusion model, production of sodium iodide aerosols and generation of the heat caused by the chemical reaction of iodine vapor and sodium vapor are taken into account in addition to the diffusion of vapor and aerosols and the heat conduction in a static spherical bubble. The diffusion of aerosols is composed of Brownian motion, thermophoresis and diffusiophoresis. In the convection model, the analysis is made for aerosol settling caused by inertial deposition, sedimentation and Brownian motion in an internal flow induced by a spherical cap bubble rising.

Increase in the initial iodine concentration in the bubble is shown to enlarge the temperature difference across a region between the reaction front and the bubble surface and enhance a contribution of thermophoresis to the aerosol diffusion through the region. The DF obtained from the calculation describes well a rapid increase at the first stage and a slow increase in the successive period, which are seen in measured DFs, and suggests the breakup of the original bubble during rising through the pool.

I. INTRODUCTION

In a postulated accident of fuel pin failure of a fast breeder reactor, fission products will be released from the failed pin to the primary cooling system including the cover gas system and further to the environment in some cases. Among the fission products, the release of iodine radioisotopes are very important for an assessment of radiological consequences due to their higher volatility and lower permissible dose to human thyroid. The released iodines are known to be retained in sodium of the cooling system in the form of sodium iodide [1]-[5], which has a little escape tendency from the sodium to the cover gas. The xenon and krypton released with iodines into the sodium pool as bubbles, however, have an influence on the reaction rate of iodine with sodium in a period of bubble rising to the pool surface. The increase in the released iodine mass will be more important to the safety assessment, to which measured release data are required to be applied.

An experimental study [6] was made to obtain the decontamination factor DF defined by the ratio of the initial iodine mass in the mixed gas bubble to the released mass into the cover gas. However, the experimental conditions were limited to the regions of higher iodine concentrations, of smaller bubble sizes and of lower sodium temperatures. A resumed work [7] was attempted to obtain the DFs and the iodine mass transfer rate from the mixed gas bubble to the liquid sodium pool under wider experimental conditions applicable to the safety assessment. In this work, the mass transfer rate was not correlated successfully with the experimental parameters due to a small number of measurements.

Therefore, experimental and analytical studies were carried out to study the mass transfer of iodine from a xenon-iodine mixed gas bubble to the liquid sodium pool.

II. EXPERIMENT

An experimental apparatus is consists of a test vessel, a damp tank of sodium, a supply system of argon and a sampling system of cover gas. The stainless steel test vessel is 0.30 m in inner diameter and 3.0 m high and contains 180 kg of sodium as shown in Fig. 1. A bubble generating device which consists of a quartz glass ball containing mixed gas of xenon-iodine and a cracking device of the ball is fixed at the bottom of the vessel. In the cover gas, a funnel device is attached on the sodium surface for collecting the mixed gas. A void sensor assembly is composed of two Chen-type sensors 0.65 mm in outer diameter. They are fastened to four arms projecting toward the center axis of the test vessel. The four assembles are attached at the positions of 0.45, 0.75, 1.05 and 1.35 m from the quartz ball in the vessel to measure the rising velocity of the mixed gas bubble.

The bubbles were generated instantaneously by cracking the quartz ball at the bottom of the vessel. The rising velocity of the bubbles was determined from the signals of the sensors arranged vertically in the sodium pool. The bubbles reaching the sodium pool surface were collected in the inverted funnel and the collected gas containing sodium iodide aerosols was carried to a vacuum vessel through aerosol filters in the sampling system as shown in Fig. 1. Materials deposited on the filters, the inner surface of the funnel, the connected pipes and the vacuum vessel were dissolved in distilled water.

The amount of iodine in the solution was determined by the use of an inductively coupled plasma mass spectrometer. The error in preparing the mixed gas concentration in the quartz ball was within ± 10 %. The measurement accuracy of the amount of iodine released into the cover gas by the processes of the sampling and the chemical analysis was less than $\pm$ 20 %. Thus, the total error accompanying each measured value was less than ± 30 %.

Experimental conditions are listed in Table 1. The size of the quartz ball was varied from 0.05 to 0.12 m in diameter and this leads to the initial bubble volume ranging from 6.5×10^{-5} to 9.0×10^{-4} m^3 which is equivalent to the fission gas volume in a fuel pin at the burn-up of 8×10^4 MWd/T. Gas pressure in the ball was adjusted to be equal to the surrounding sodium pressure. The cover gas

pressure was maintained at the atmospheric pressure during the experiment. The initial iodine concentration in the ball ranged from 1.0 to 40.0 mol%. Among the values, 4.0 mol% is equivalent to the fraction of iodine produced at the burn-up of 8 x 10^4 MWd/T. The sodium pool temperature was varied in the range from 573 to 873 K, since the temperature of 773 K is equivalent to the sodium coolant temperature. The sodium pool depth was also changed from 0.03 to 2.0 m to vary the bubble rise time.

III. EXPERIMENTAL RESULTS AND DISCUSSION

1. Bubble Rise in Sodium Pool

Figure 2 shows the results for the bubble rising process with the parameter of the initial bubble volume. It is found in Fig. 2 that the bubbles rise linearly with time except for the initial period. The rising velocity of the bubble is also found to increase with an increase in the initial bubble volume. These facts indicate that the bubble comes up to the sodium surface at a terminal velocity.

Shapes of the rising bubble has been characterized by non-dimensional numbers [8] : Eotvos number Eo, Morton number M, and Reynolds number Re. By the use of the terminal velocity obtained from the results in Fig. 2 and the ball diameter d_e, the numbers are calculated to be in the range of Eo = 130 ~ 740, M = 1.11x10^{-14} and Re = 7.27x10^4 ~ 2.60x10^5. In accordance with the shape regimes for bubbles given by Crift, et al. [9], these values indicate that the bubbles are in the shape of spherical cap in the present experiment. The terminal velocity of the spherical cap-shaped bubble was given by Crift, et al. [10] in the expression

$$U_T = 0.711\{g\, d_e (\rho_l - \rho_b) / \rho_l\}^{1/2} \qquad (1)$$

The terminal velocity U_T was calculated on the assumption that the bubble has an equivalent volume to that of the quartz ball. The results are shown with a thick line in Fig. 3. It is found in Fig. 3 that the measured velocities are lower than the calculated line and the difference becomes larger with increasing the initial bubble volume. This implies that the bubble broke up into several smaller bubbles during the rising period.

The behavior of the rising bubble was visualized in a water pool, which was 0.30 m long, 0.30 m wide and 1.50 m deep. The bubbles were generated by cracking a quartz ball containing air quite similarly to the experiment in the sodium pool. The water experiments were performed under the conditions where the range of the non-dimensional numbers were equivalent to those in the sodium experiments. Photo. 1 shows a series of photographs of the rising bubble at 0.1, 0.3, 0.5 and 1.0 s after cracking the quartz ball in the water pool. The breakup of bubble into smaller bubbles and forming the spherical cap are observed in the photographs.

Therefore, the difference between measured and calculated terminal velocities can be attributed to the bubble breakup into smaller spherical cap-shaped bubbles.

2. Iodine Mass Transfer from Bubble to Sodium Pool

Since the bubble breakup into smaller bubbles is observed in the present experiment, the transferred iodine mass per the unit initial bubble volume is used instead of that per the unit surface area of the bubble. Figure 4 shows the results for the transferred iodine mass against the bubble rise time on the log-log graph with the parameter of the initial iodine concentration. It is found in Fig. 4 that the transferred mass increases with the time and shifts to the larger values with increasing initial iodine concentration. Figures 5 and 6 show the results for the transferred iodine mass per the unit initial bubble volume with the parameters of the initial bubble volume and the sodium temperature,

respectively. It is noticed in these figures that the transferred mass are not sensitive to the changes in the initial bubble volume and the sodium temperature.

Linear relations are observed between the transferred mass and the time on the log-log graphs. By the use of the method of least squares, the transferred iodine mass Q can be given as a function of the time t in the form

$$Q = a\,t^{b} \qquad (2)$$

where a and b are constants. The relations are shown with the linear lines in Figs. 4, 5 and 6. A time-dependent mass transfer rate is obtained by differentiating Eq. (2) with respect to t and the results are shown with the parameter of the initial iodine concentration in Fig. 7. Figure 7 indicates that the mass transfer rates decrease rapidly from large values just after the bubble generation and do slowly for successive period shifting to higher values with increasing the iodine concentration.

A decontamination factor DF defined by the ratio of the iodine mass in the initial gas bubble over that released into the cover gas was calculated from the experimental results and the calculated DFs are shown in Fig. 8. It is seen in Fig. 8 that the DFs trend to increase rapidly just after the bubble generation and to increase slowly for the successive period, while the DFs depend on the iodine concentration.

The DFs were determined in another way, where the iodine mass released into the cover gas was calculated by subtraction of a sum of the present mass transfer rate multiplied by each time section from the iodine mass in the initial gas bubble. The calculated DFs are shown by curved lines in Fig. 8. These curved lines appear to describe well qualitatively the dependence of DFs on time and on the initial iodine concentration. However, the description of the rapid increase just after the bubble generation and of the slow increase for successive period is not successful. This implies that an analysis based on more mechanistic models is required for the precise prediction of the DF for a long period as well as just after the bubble generation.

IV. ANALYTICAL MODELS

1. Models and Assumptions

Based on the observations of the bubble rising through the sodium pool and the simulated water pool, analytical models are constructed for the mass and heat transfer in the xenon-iodine mixed gas bubble as shown in Fig. 9 and explained below.

(1) The bubble is static and spherical within an initial short period just after the bubble generation. In the static spherical bubble, the mass transfer is controlled by diffusion and the heat transfer by conduction and radiation which is named as a diffusion model.

(2) The bubble becomes a form of spherical cap during rising through the pool. In the spherical cap type bubble, the mass transfer is governed by the internal flow of the mixed gas induced by the bubble rising which is named as a convection model.

The following assumptions are used in the models.

(a) For the diffusion model, the iodine vapor is uniformly distributed in the bubble at the initial stage.

(b) The sodium vapor evaporated on the interface of the bubble and sodium is in saturation at the surface temperature.

(c) The iodine vapor reacts with sodium vapor on a spherical reaction front generating the heat of reaction and sodium iodide, which instantaneously forms aerosols of 0.1 μ m in mass-median diameter as generally seen in other combustion products [11].

(d) The size of the spherical bubble and the pressure of the mixed gas bubble do not change in the consequence of the chemical reaction.

(e) The aerosols settle on the bubble surface by diffusion composed of Brownian motion, thermophoresis and diffusiophoresis during the initial short period.

(f) The gradient of aerosol concentration between the reaction front and the bubble surface in approximately proportional to those of sodium concentration and temperature.

(g) For the convection model, the aerosol settling is enhanced by the convective flow in the rising bubble. Inertial deposition and sedimentation are considered in the settling as well as that by Brownian motion.

2. Diffusion Model

(1) Diffusion and Energy Equations

The mass transfer in the static bubble is expressed by the equation of mass conservation in the spherical coordinate

$$\partial C / \partial t = D (\partial^2 C / \partial r^2 + 2 / r \cdot \partial C / \partial r) \qquad (3)$$

and the heat transfer by the equation of energy conservation

$$\partial T / \partial t = \kappa \ (\partial^2 T / \partial r^2 + 2 / r \cdot \partial T / \partial r). \qquad (4)$$

The initial concentrations of iodine and sodium and the initial temperatures of xenon-iodine and xenon-sodium mixed gas as written as

$$C_I = C_0,$$
$$C_S = C_R,$$
$$T_{XI} = T_0,$$
$$T_{XS} = T_R,$$

inside the bubble. The reaction front moves with time from the bubble surface toward the bubble center and generates the heat of reaction and the sodium iodide aerosols. The generation rate of the aerosols depends on the reaction rate. The equations subjected to these conditions can not be solved in an analytical form. Thus, the equation should be determined by a sequential connection method where the analytical solution for a short time section was connected to that for the next time section sequentially by substitution of the resultant concentration profile and temperature profile at the time section Δt for the initial ones in the next time section.

The equation of diffusion is applied to the iodine transfer in the core region inside the reaction front in the bubble. The initial and boundary conditions in the time section are given as

$$C_I = f_I(r) \text{ for } 0 < r \leqq r_f \text{ when } t^* = 0, \ (t \leqq t^* \leqq t + \Delta t)$$
$$C_I = 0 \quad \text{for } t^* > 0 \quad \text{at} \quad r = r_f,$$

where $f_I(r)$ designates the initial concentration profile of iodine vapor as a function of the radius r from the center of the bubble, and r_f is the radius of the reaction front.

The equation of diffusion is also applied to the sodium transfer in the region between the reaction front and the bubble surface. The initial and boundary conditions in the time section are given as

$$C_S = f_S(r) \text{ for } r_f \leqq r \leqq R \text{ when } t^* = 0, \ (t \leqq t^* \leqq t + \Delta t)$$

$$C_S = C_R \quad \text{for } t^* > 0 \quad \text{at} \quad r = R,$$
$$C_S = 0 \quad \text{for } t^* > 0 \quad \text{at} \quad r = r_f,$$

where $f_S(r)$ designates the initial concentration profile of sodium and R is the radius of the bubble surface.

The mass balance in the chemical reaction is expressed as

$$Na + 1/2\, I_2 = NaI + \Delta H^0 T_f, \tag{5}$$

where $\Delta H^0 T_f$ is the standard enthalpy of formation at temperature T_f [12]. Equation (5) yields the relation between fluxes of iodine and sodium at the reaction front as

$$-2 D_{XI}\, \partial C_I / \partial r \,|_{r=r_f} = D_{XS}\, \partial C_S / \partial r \,|_{r=r_f}, \tag{6}$$

where D_{XI} and D_{XS} are the diffusion coefficients of iodine vapor and sodium vapor in xenon, respectively [13]. The unknown variable r_f can be determined by equating both sides of Eq.(6).

The equation of heat conduction is applied to the heat transfer in the core region inside the reaction front. The initial and boundary conditions in the time section are written as

$$T_{XI} = g_{XI}(r) \text{ for } 0 < r \leqq r_f \text{ when } t^* = 0, \quad (t \leqq t^* \leqq t + \Delta t)$$
$$T_{XI} = T_f \quad \text{for } t^* > 0 \quad \text{at} \quad r = r_f,$$

where $g_{XI}(r)$ designates the initial temperature profile in the core region.

The initial and boundary conditions in the time section in the region between the reaction front and the bubble surface are written as

$$T_{XS} = g_{XS}(r) \text{ for } r_f \leqq r \leqq R \text{ when } t^* = 0, \quad (t \leqq t^* \leqq t + \Delta t)$$
$$T_{XS} = T_R \quad \text{for } t^* > 0 \quad \text{at} \quad r = R,$$
$$T_{XS} = T_f \quad \text{for } t^* > 0 \quad \text{at} \quad r = r_f.$$

In these equations, $g_{XS}(r)$ is temperature profile in the region and T_f and T_R are temperatures at the reaction front and at the bubble surface.

The heat of reaction generated at the reaction front is given from Eq. (5) as

$$Q_f = -2 \Delta H^0 T_f N_{I,\, r=r_f} = \Delta H^0 T_f N_{S,\, r=r_f}, \tag{7}$$

where $N_{I,\, r=r_f}$ and $N_{S,\, r=r_f}$ are the mass flux of iodine and that of sodium at the reaction front, respectively. This reaction heat is transferred to the core region inside the reaction front and to the region between the reaction front and the bubble surface as

$$\begin{aligned} Q_f = {} & \lambda_{XI}\, \partial T_{XI} / \partial r \,|_{r=r_f} - \lambda_{XS}\, \partial T_{XS} / \partial r \,|_{r=r_f} \\ & + F_{fR}\, \sigma (T^4_f - T^4_R) - N_{I,\, r=r_f} C_{p,I} (T_f - T_{XI}) \\ & - N_{S,\, r=r_f} C_{p,S} (T_R - T_f) + N_{SI,\, r=r_f} C_{p,SI} (T_f - T_R), \end{aligned} \tag{8}$$

where λ_{XI} and λ_{XS} are thermal conductivities in each region [14], F_{fR} is radiative heat transfer coefficient between the reaction front and the bubble surface [15], $C_{p,I}$, $C_{p,S}$ and $C_{p,SI}$ are specific heats [16], and σ is the Stefan-Boltzmann constant. The first term of the right-hand side of Eq.(8) represents the heat flux of conduction at the reaction front toward the center of the bubble. The second and third terms represent those of conduction and radiation at the reaction front toward the bubble surface. The remaining three terms represent the transferred heats due to the mass transfer of iodine vapor, sodium vapor and sodium iodide aerosols, respectively. The temperatures in Eq.(8) are given by the solutions of the equation of heat conduction.

The heat balance at the bubble surface is expressed as

$$\begin{aligned} &- \lambda_S \, \partial T_S / \partial r \,|_{r=R} - N_{S,\, r=r_f} \Delta H_v \\ &= \lambda_{XS} \, \partial T_{XS} / \partial r \,|_{r=R} + F_{fR} \, \sigma \, (T^4_f - T^4_R) \\ &\quad - N_{S,\, r=R} \, C_{p,S} \, (T_R - T_f) + N_{SI,\, r=R} \, C_{p,SI} \, (T_f - T_R), \end{aligned} \tag{9}$$

where λ_S and ΔH_v are the thermal conductivity and the evaporation heat of liquid sodium [17], $N_{S,\, r=r_f}$ and $N_{SI,\, r=R}$ are the mass flux of sodium and that of sodium iodide at the bubble surface, respectively. The left-hand sides of Eq.(9) express heat conduction into the sodium pool and heat of evaporation of sodium at the bubble surface. The two unknown variables T_f and T_R are determined by solving Eq.(8) and Eq.(9) simultaneously.

(2) Aerosol Diffusion in Region between Reaction Front and Bubble Surface

Sodium iodide aerosols generated at the reaction front will be transferred inside and outside it in the proportion of velocity vectors for the Brownian motion [18] v_{BD}, thermophoresis [19] v_{TP}, and diffusiophoresis [20] v_{DP}, The resultant flux of the aerosols at the reaction front toward the bubble surface $N_{SI,\, r=r_f}$ is determined from the equation

$$\begin{aligned} N_{SI,\, r=r_f} = &-N_{S,\, r=r_f} (v_{BD,R} + v_{TP,R} + v_{DP,R}) \\ &/ \{(v_{BD,R} + v_{TP,R} + v_{DP,R}) + (v_{BD,C} + v_{TP,C} + v_{DP,C})\}. \end{aligned} \tag{10}$$

As the aerosol concentration profile is observed to be almost linear in the region between the reaction front and the bubble surface, the apparent diffusion coefficient of the aerosols is used so as to simplify the calculation of aerosol diffusion. The apparent diffusion coefficient D_{SI} is expressed as

$$D_{SI} = (v_{BD,R} + v_{TP,R} + v_{DP,R}) (R - r_f). \tag{11}$$

In the calculation of the velocity vectors in Eqs. (10) and (11), physical properties of the gas and aerosols are given as estimated values calculated from theoretical equations [14],[16].

The initial and boundary conditions in the time section in the aerosol diffusion through the region between the reaction front and the bubble surface are

$$\begin{aligned} &C_{SI} = f_{SI}(r) && \text{for } r_f \leqq r \leqq R \text{ when } t^* = 0, \ (t \leqq t^* \leqq t + \Delta t) \\ &- D_{SI} \, \partial C_{SI} / \partial r = N_{SI,\, r=r_f} && \text{for } t^* > 0 \quad \text{at} \quad r = r_f, \\ &C_{SI} = 0 && \text{for } t^* > 0 \quad \text{at} \quad r = R, \end{aligned}$$

where $f_{SI}(r)$ designates the initial concentration profile of sodium iodide aerosols. The decontamination factor DF is determined from the initial amount of iodine in the bubble $[M_I]_{t=0}$ and the total amount of iodine vapor and that of sodium iodide aerosols

$$DF = [M_I]_{t=0} / (4\pi \int_0^{rf} C_I r^2 dr + 2\pi \int_{rf}^{R} C_{SI} r^2 dr). \quad (12)$$

3. Convection Model

The equation of motion describing the bubble rising through a liquid pool is expressed by the terms of the inertia, buoyancy and drag force as [21]

$$4/3\ \pi r_e^3 (\rho_b + 1/2\ \rho_s)\ \partial U_b / \partial t$$
$$= 4/3\ \pi r_e^3 (\rho_s - \rho_b) g - C_D (\pi r_e^2) / 2\ \rho_s U_b^2, \quad (13)$$

where U_b is the rising velocity of the bubble, r_e the radius of sphere having a volume equal to the bubble and C_D the drag coefficient, and ρ_b and ρ_s are the densities of bubble and liquid sodium, respectively. The values of r_e and C_D are calculated in consideration of deformation [22] and expansion [23] of the bubble during the rising.

The settling coefficients, which are defined by the ratio of a number of aerosols deposited on the bubble surface per unit rise path to a total number of those in the bubble, are given for the inertial deposition α_{ID}, for the sedimentation α_{SD} and for the diffusion α_{BD} by [24]

$$\alpha_{ID} = 9\ U_b\ \tau / (2 r_e^2), \quad (14)$$
$$\alpha_{SD} = 3\ g\ \tau / (4 r_e U_b), \quad (15)$$
$$\alpha_{BD} = 1.8\ (D_{SI})^{1/2} / (U_b r_e^3)^{1/2}, \quad (16)$$

where τ is the relaxation time [25]. The decrease in aerosol concentration with time ΔC_{SI} is given by summing up the contributions of these processes as

$$\Delta C_{SI} = (\alpha_{ID} + \alpha_{SD} + \alpha_{BD})\ U_b\ C_{SI}. \quad (17)$$

The decontamination factor DF in the n-th time section Δt_n is given by

$$DF = 2\ [M_I]_{t=0} / ([M_{SI}]_{t=\Delta tn-1} - V_b\ \Delta C_{SI}\ \Delta t_n, \quad (18)$$

where V_b is the bubble volume.

V. CALCULATED RESULTS AND DISCUSSION

1. Diffusion Process in Spherical Bubble

(1) Concentration and temperature profiles

Figure 10 shows the concentration profiles of iodine, sodium and sodium iodide and a temperature

profile at 0.1 s after the bubble generation with 4 mol% for the initial iodine concentration. It is observed from the concentration profiles that the vapors of iodine and sodium diffuse to the reaction front where both the concentrations are kept zero, and the aerosols of sodium iodide generated at the front diffuse mainly toward the bubble surface. The temperature profile shows that the heat of reaction transfers from the front to the inside of the bubble and the bubble surface.

(2) Temperature rise at reaction front and its size

The temperature difference across the region between the reaction front and the bubble surface is calculated as a function of time and the results are shown with the parameter of the initial concentration in Fig. 11. The temperature difference is seen to have its peak value just after the bubble generation and to increase as the initial concentration increases. This is because the heat generation rate at the reaction front increases with the higher iodine concentration.

The radius of the reaction front is shown with the parameter of the initial concentration in Fig. 12. It is found in Fig. 12 that the reaction front moves toward the bubble center and this movement is reduced in the case of the higher iodine concentration.

(3) Residual amount of iodine and sodium iodide in the bubble

The residual amount of iodine in the bubble is calculated by integrating the iodine concentration with respect to the radius, and shown in Fig. 13 with the parameter of the initial iodine concentration. Through the similar procedure, the amount of sodium iodide in the bubble is shown in Fig. 14. It is found in Figs. 13 and 14 that with increasing the initial concentration, the curve of the residual amount of iodine shifts to a higher level whereas that of sodium iodide does to a lower level. The increase in the residual amount of iodine is simply attributed to the higher iodine concentration in the bubble. To understand the reason for the decrease in the amount of sodium iodide, an analysis is made for the aerosol diffusion in the bubble. The velocity vectors of the Brownian motion, thermophoresis and diffusiophoresis are tabulated in Table 2 under the initial iodine concentration of 4 and 40 mol%. Table 2 indicates that the thermophoresis contributes largely to the aerosol diffusion across the region between the reaction front and the bubble surface and that the diffusiophoresis does to the reaction front. The enlarged temperature difference between the narrower region, which are caused by the higher iodine concentration, enhances the thermophoresis and increases the amount of aerosol deposition on the bubble surface. The reason for the decrease in the amount of sodium iodide with increasing the initial iodine concentration can be interpreted by this process.

(4) Comparison of calculated DF with measured DF

Figure 15 through 18 show the results for the DFs calculated and measured under the initial iodine concentration of 4, 8, 20 and 40 mol% with lines and marks respectively. The parameter in the calculation is the diameter of spherical bubble. In the measurement, a quartz ball containing xenon-iodine mixed gas was cracked at the bottom of a sodium pool to generate the initial bubble. The size of the quartz ball is 0.1 m. The measured DFs lie between the curves of calculated DF with the bubble diameter of 0.03 m and 0.01 m. The breakup of an initial bubble into several bubbles about 0.03 m in diameter and many fine bubbles about 0.01 m in diameter is observed in photographs taken in the air bubble rising through a water pool. The measured DFs being between the two curves can be explained by this bubble breakup process, and two steps of increase in the measured DFs with time is well described by the change in the calculated DFs.

2. Convection Process in Spherical Cap Bubble

The DFs calculated for the convection process under the initial iodine concentration of 4, 8, 20 and 40 mol% and the aerosol diameter of 0.1 μ m are shown with lines in Figs. 15 through 18,

respectively. The DFs measured under the initial iodine concentration are also shown with symbols in these figures. The parameter in the figure is the initial diameter of the spherical bubble. It is found in these figures that the DF curve shifts to the lower level with enlarging the bubble diameter and that the measured DFs are between two DF curves obtained from the bubble diameter of 0.03 and 0.01 m with some exceptions.

VI. CONCLUSIONS

The following conclusions are obtained from the experimental study.

(1) The difference in the predicted and measured bubble rise velocities indicates that the original bubble have been broken up into several smaller bubbles of spherical cap type during the rising period. Observation of bubble rising through the water pool supports the bubble breakup into smaller spherical bubbles.

(2) The transferred iodine mass per the unit initial bubble volume from the bubbles to the sodium pool is well correlated with the bubble rise time and the experimental conditions. The correlation shows that the transferred mass increases with the time shifting to a large value as the initial iodine concentration increases and is not sensitive to the changes in the initial bubble volume and the sodium temperature.

(3) The mass transfer rate determined by differentiating the empirical equation of the transferred mass with respect to the time describes the dependency of the iodine transfer on the time and the initial iodine concentration.

(4) The measured decontamination factors show a rapid increase just after the bubble generation and a slow increase for the successive period.

(5) The decontamination factor calculated by the use of the mass transfer rate describes quantitatively the increase in the measured decontamination factors with increasing the bubble rise time and the initial iodine concentration. For the precise description of the DF, an analysis based on more mechanistic models is required.

From the analytical study, the following conclusions are obtained.

(1) The increase in the initial iodine concentration increases the heat generation at the reaction front to raise the temperature at the front. The enlarged temperature difference across the region between the reaction front and the bubble surface greatly enhances the contribution of the thermophoresis to the deposition of sodium iodide aerosols on the bubble surface.

(2) The decontamination factor DF calculated on the basis of the diffusion model in the spherical bubble describes well the rapid increase in the measured DFs in the first stage and their positive shift with the initial iodine concentration.

(3) The breakup of original bubble into small bubbles during rising through the sodium pool is consistent with the fact that the measured DFs being between the DF curves with the bubble diameter of 0.03 m and 0.01 m.

(4) The DF curve calculated on the basis of the convection model in the spherical cap bubble describes the slow increase in the measured DFs in the successive period.

[NOMENCLATURE]

C : Concentration (mol/m^3) or (mol%)

C_D : Drag coefficient

C_p : Specific heat at constant pressure (kJ/mol-deg)

D : Mass diffusivity (m^2/s)

d_e : Spherical bubble diameter (m)

Eo : Eotvos number (= $g (\rho_l - \rho_b) d_e^2 / \sigma$)

F : Radiative heat transfer coefficient

g : Gravitational acceleration (m/s^2)

L_s : Sodium pool depth (m)

M : Morton number ($= g\mu^4 (\rho_l - \rho_b) / \rho_l^2 \sigma^3$) or Mass (mol)

N : Mass flux (mol/m^2s)

Q : Transferred iodine mass per unit initial bubble volume from bubble to sodium pool (mol/m^3) or Heat flux (kJ/m^2s)

Q' : Mass transfer rate of iodine per unit initial bubble volume from bubble to sodium pool (mol/m^3s)

R : Radius of spherical bubble (m)

Re : Reynolds number ($= d_e U/\mu$)

r : Radius in spherical coordinate (m)

T : Temperature (K)

t : Time (s)

t* : Modified time (s)

U_b : Bubble rising velocity (m/s)

U_T : Terminal velocity of rising bubble (m/s)

V_b : Bubble volume (m^3)

v : Velocity vector of aerosol diffusion (m/s)

α : Settling coefficient of aerosol

$\Delta H^0_{T_f}$: Standard enthalpy of sodium iodide formation at temperature T_f in Eq. (5) (kJ)

ΔH_v : Evaporation heat of liquid sodium (kJ/mol)

μ : Viscosity of liquid (kg/m-s)

ρ_b : Density of gas bubble (kg/m^3)

ρ_l : Density of liquid (kg/m^3)

σ : Surface tension of liquid (kg/s^2)

κ : Thermal diffusivity (m^2/s)

λ : Thermal conductivity (kJ/m-s-deg)

τ : Relaxation time (s)

(Subscript)

0 : Initial

b : Bubble

BD : Brownian diffusion

C : Bubble center

DP : Diffusiophoresis

f : Reaction front

I : Iodine

ID : Inertial deposition

R : Bubble surface

S : Sodium

SD : Sedimentation

SI : Sodium iodide

TP : Thermophoresis

XI : Xenon-iodine mixed gas

XS : Xenon-sodium mixed gas

ACKNOWLEDGMENT

The authors wish to express their appreciation to Mr. H. Tanabe, and Mr. O. Miyake, Plant Safety Section (PSS), Safety Engineering Division (SED), Oarai Engineering Center (OEC), PNC, for valuable discussion given to the present work and to the members of Source Term Research Group of PSS for their powerful assistance. The authors gratefully acknowledge the supports of Ms. K. Akiyama and Ms. M. Isozaki, PSS/SED/OEC/PNC, in typing and drawing this paper.

REFERENCES

[1] Kunkel,W.P.: NAA-SR-11766, (1966).
[2] Clough,W.S.: J. Nucl. Energy, 21[3], 225 (1967).
[3] Castleman,A.W., Tang,I.N.: Nucl. Sci. Eng., 29[2], 159 (1967).
[4] Kieholtz,G.W., Battle,G.C.: ORNL-NSIC-37, (1969).
[5] Smith,R.R., et al.: Trans. Amer. Nucl. Soc., 10[2], 634 (1969).
[6] Nelson,C.T., et al.: Proc. Int. Mtg. Fast Reactor Safety and Related Physics, Chicago, USA, 1937 (1976).
[7] Miyahara,S., Shimoyama,K.: Proc. Int. Seminar "Liquid Metal Systems - Material Behavior and Physical Chemistry in Liquid Metal Systems II", Plenum Press, 27 (1995).
[8] Crift,R., Grace,J.R., Weber,M.E.: "Bubbles, Drops, and Particles", Academic Press, 26 (1978).
[9] Crift,R., Grace,J.R., Weber,M.E.: ibid., 27 (1978).
[10] Crift,R., Grace,J.R., Weber,M.E.: ibid., 205 (1978).
[11] Takahashi,K.: "Kiso Earozoru Kougaku" (Fundamental Aerosol Technology), Yohkendoh, Tokyo, 4 (1982) [in Japanese].
[12] Charse,Jr.M.W., et al.: "JANAF Thermochemical Tables", (3rd ed.) Am. Chem. Soc. and Am. Inst. of Phys., (1985).
[13] Slattery,J.C.,Bird,R.B.: A.I.Ch.E.J., 4, 137-142 (1958).
[14] Reid,I.C., et al.: "The Properties of Gases and Liquids", (3rd ed.) McGraw-Hill, (1977).
[15] Shire,P.R.: "SPRAY CODE USER's REPORT", HEDL-TME 76-94, 34 (1977).
[16] Barin,I.,Knacke,O.: "Thermochemical properties of inorganic substances", Springer-Verlag, (1973).
[17] Foust,O.J.: "SODIUM-NaK ENGINEERING HANDBOOK", Gordon and Breach, Sci. Publ., (1972).
[18] Einstein,A.: Ann. Phys. 17, 549 (1905).
[19] Brock, J.R.: J. Colloid Sci., 17, 768 (1962).
[20] Waldmann,L.: Z. Naturfolsch, 14A, 589 (1959).
[21] Crift,R.,Grace,J.R.,Weber,M.E.: "Bubbles, Drops, and Particles", Academic Press, 317 (1978).
[22] Powers,D.A.,Sprung,J.L.: "A Simplified Model of Aerosol Scrubbing by a Water Pool Overlying Core Debris Interacting with Concrete", NUREG/CR-5901, 7-9 (1993).
[23] Rayleigh,L.,: Phil. Mag., [34], 94 (1917).
[24] Fuchs,N.A.: "The Mechanics of Aerosols", Pergamon Press, 242-243 (1964).
[25] Fuchs,N.A.:ibid., 71 (1964).

Table 1 Experimental Conditions

Quartz Ball Diameter (m)	0.05 , 0.07 , 0.1 , 0.12
Initial Bubble Volume ($\times 10^{-4} m^3$)	0.65 , 1.8 , 5.2 , 9.0
Initial Iodine Concentration (mol%)	1.0 , 4.0 , 8.0 , 20.0 , 40.0
Sodium Pool Temperature (K)	573 , 673 , 773 , 873
Sodium Pool Depth (m)	0.03 , 0.25 , 0.5 , 1.0 , 1.5 , 2.0

Table 2 Velocity vectors of aerosol diffusion at reaction front (at 0.1s)
Sodium pool temperature : 773K
Bubble diameter : 0.03m
(facing bubble surface is denoted as plus)

Velocity Vector	Initial Iodine Concentration	
	4mol%	40mol%
$\mathcal{V}_{BD,R}$	1.253×10^{-6} (m/s)	1.113×10^{-5} (m/s)
$\mathcal{V}_{TP,R}$	5.263×10^{-3} (m/s)	1.484×10^{-1} (m/s)
$\mathcal{V}_{DP,R}$	-2.464×10^{-4} (m/s)	-2.685×10^{-3} (m/s)
$\mathcal{V}_{BD,c}$	-3.707×10^{-8} (m/s)	-5.171×10^{-8} (m/s)
$\mathcal{V}_{TP,c}$	-2.893×10^{-4} (m/s)	-1.380×10^{-3} (m/s)
$\mathcal{V}_{DP,c}$	5.030×10^{-4} (m/s)	8.865×10^{-3} (m/s)

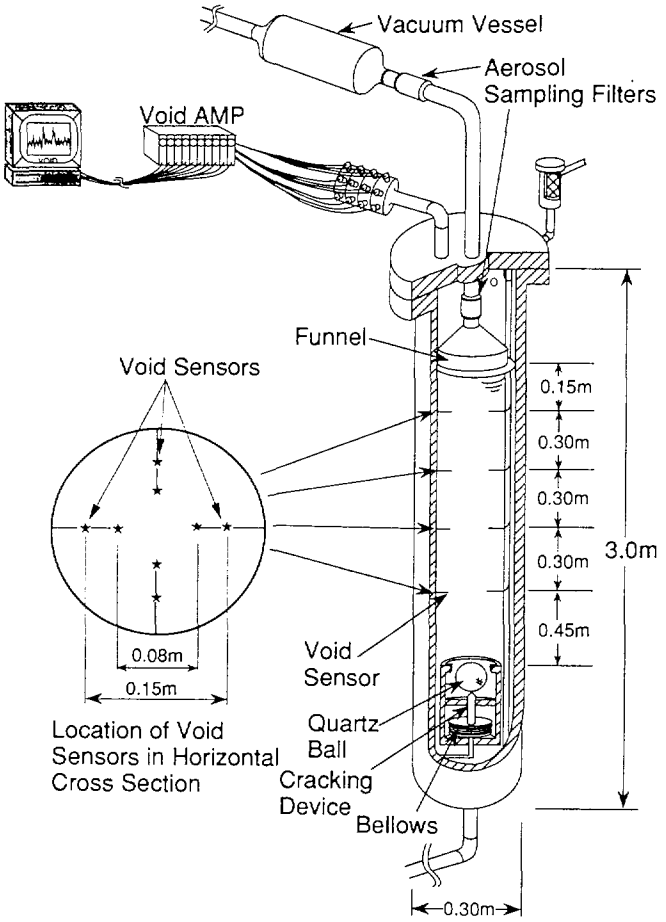

Fig.1 Arrangement of test vessel and location of void sensors

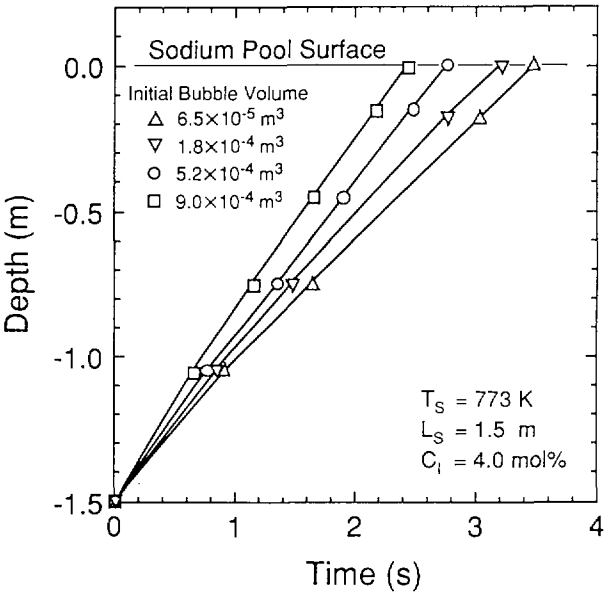

Fig.2 Bubble rising process

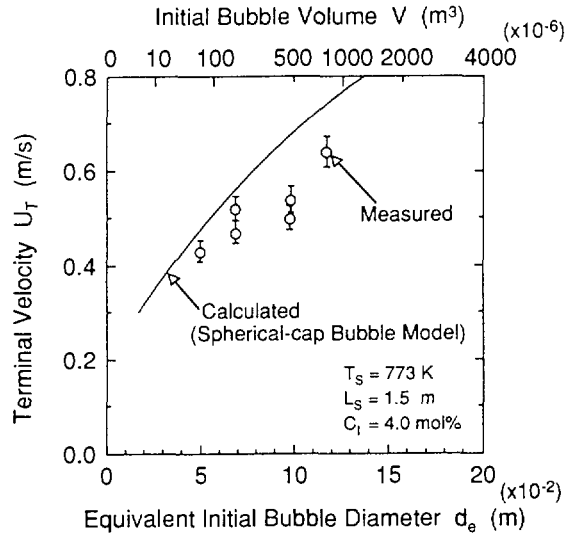

Fig.3 Terminal velocity of bubbles measured and calculated

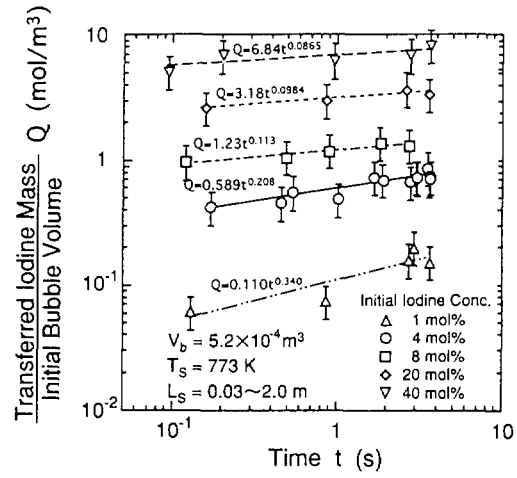

Fig.4 Effect of initial iodine concentration on transferred iodine mass into sodium

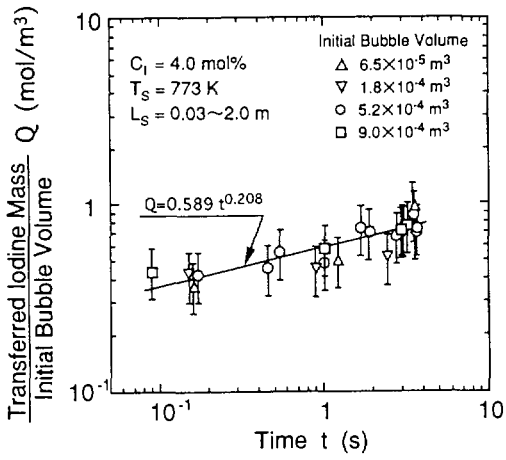

Fig.5 Effect of initial bubble volume on transferred iodine mass into sodium

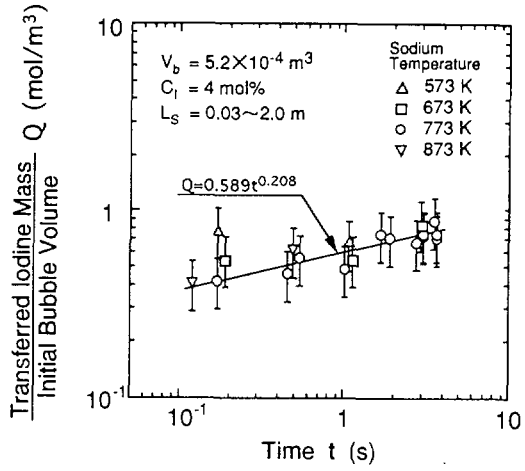

Fig.6 Effect of sodium temperature on transferred iodine mass into sodium

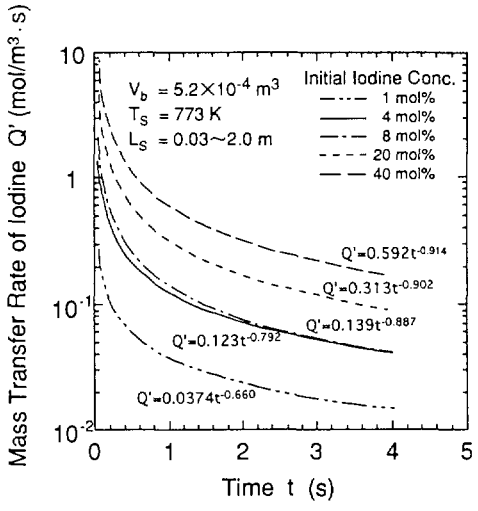

Fig.7 Effect of initial iodine concentration on mass transfer rate

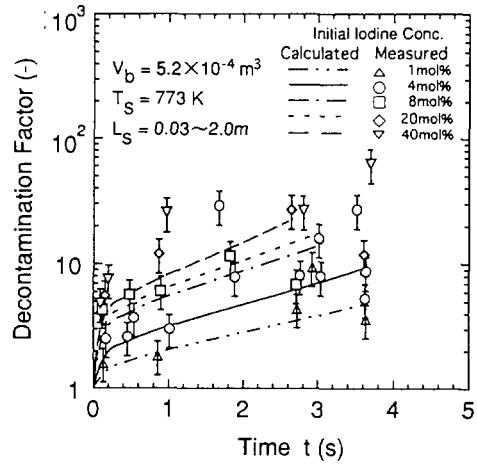

Fig.8 Decontamination factor of iodine in bubbles

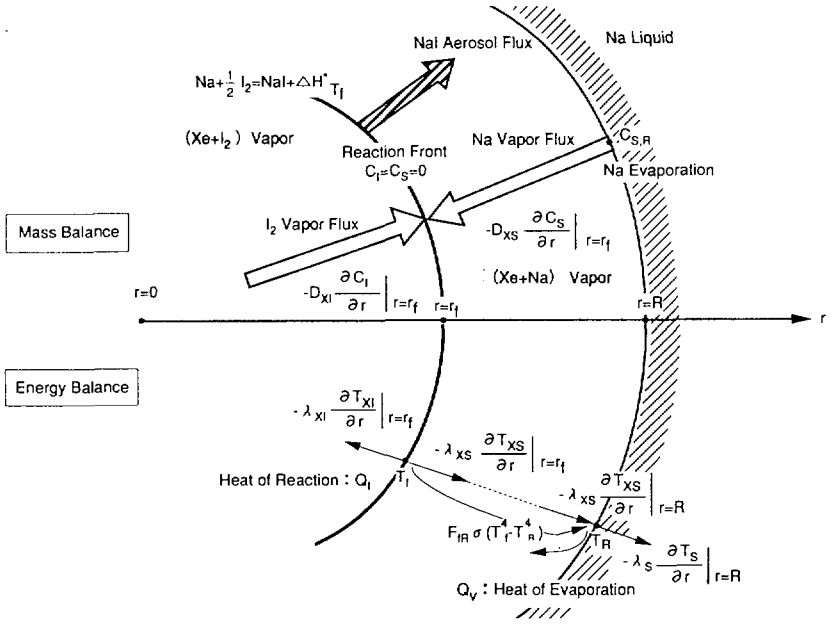

Fig.9 Mass and heat transfer in spherical, xenon-iodine mixed gas bubble

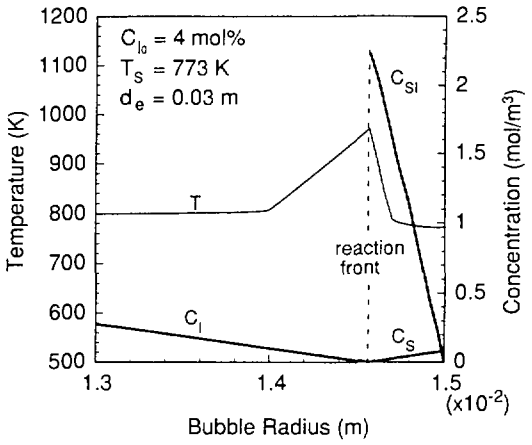

Fig.10 Profiles of temperature and concentration in spherical bubble (at 0.1s)

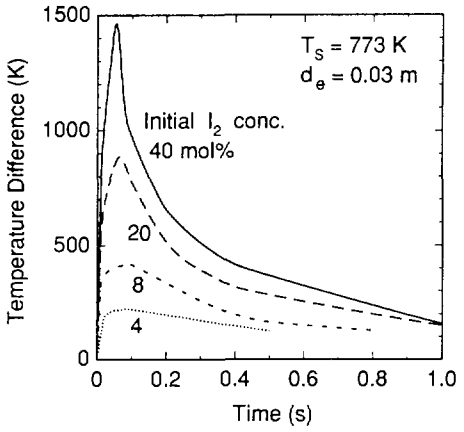

Fig.11 Temperature difference across region between reaction front and bubble surface increasing with initial Iodine concentration

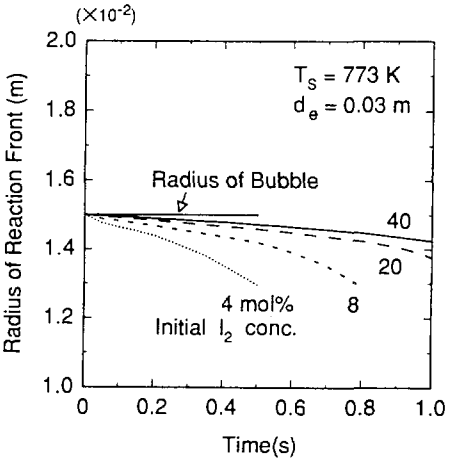

Fig.12 Radius of reaction front decreasing with initial iodine concentration

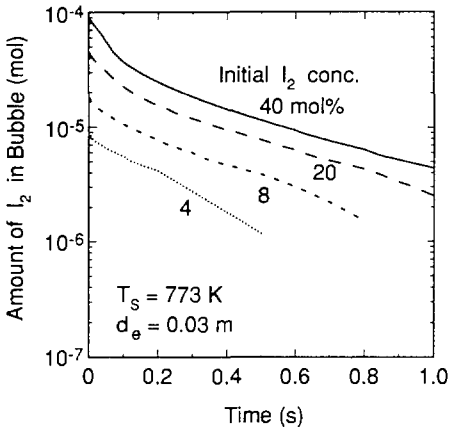

Fig.13 Amount of iodine in bubble increasing with initial iodine concentration

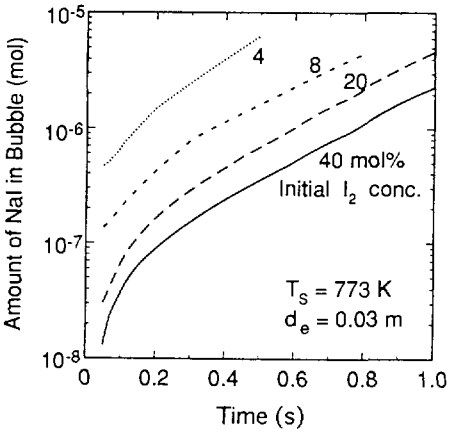

Fig.14 Amount of sodium iodide in bubble decreasing with initial iodine concentration

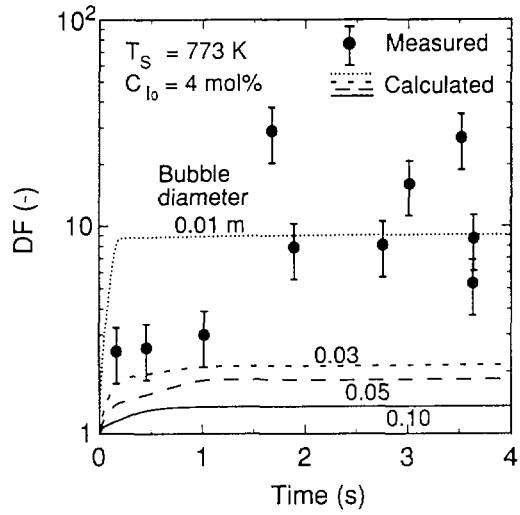

Fig.15 Calculated and measured DFs at initial iodine concentration of 4mol%

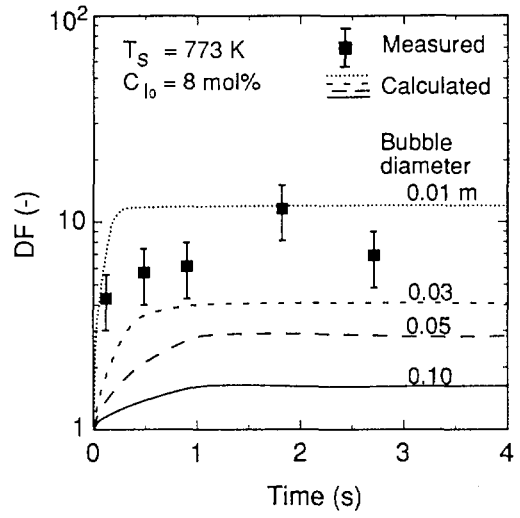

Fig.16 Calculated and measured DFs at initial iodine concentration of 8mol%

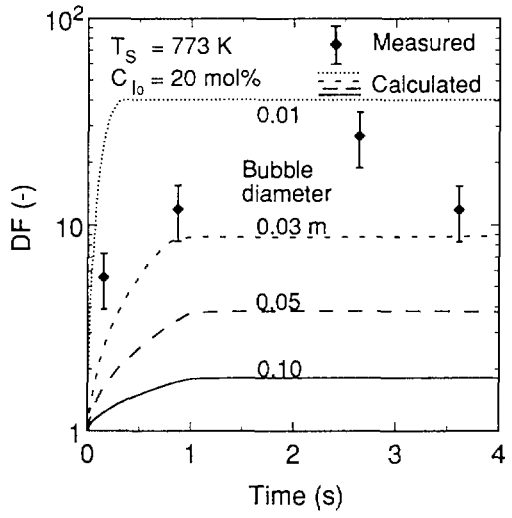

Fig.17 Calculated and measured DFs at initial iodine concentration of 20mol%

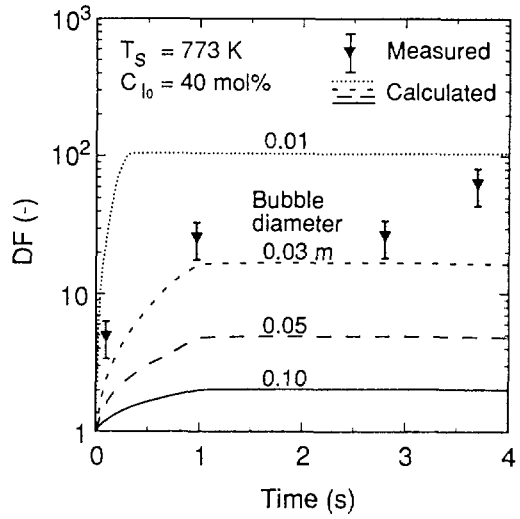

Fig.18 Calculated and measured DFs at initial iodine concentration of 40mol%

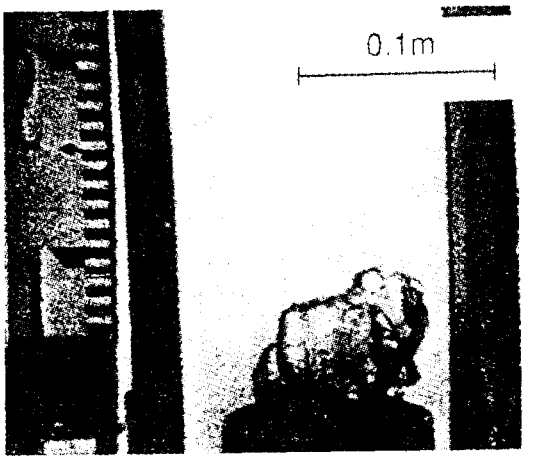

(1) 0.1 s after cracking quartz ball 0.1 m in diameter

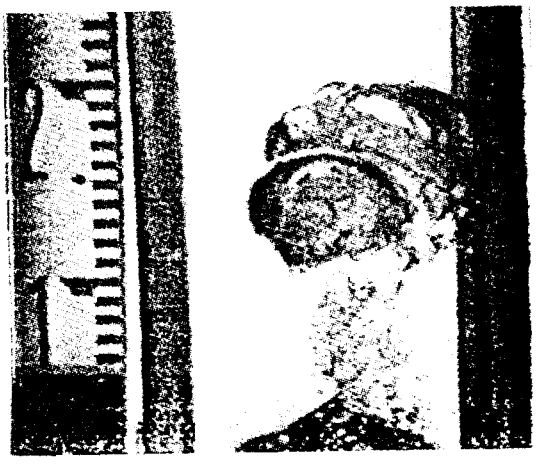

(2) 0.3 s after the cracking

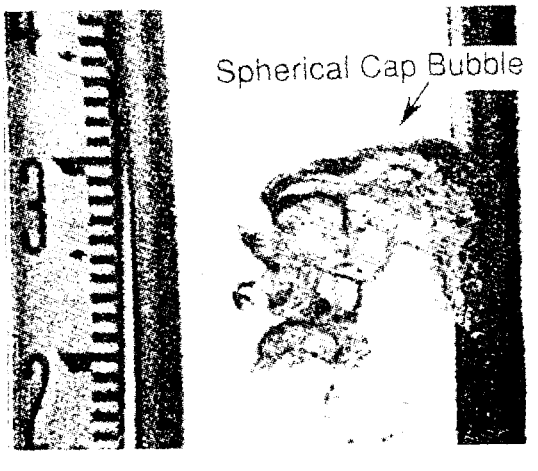

(3) 0.5 s after the cracking

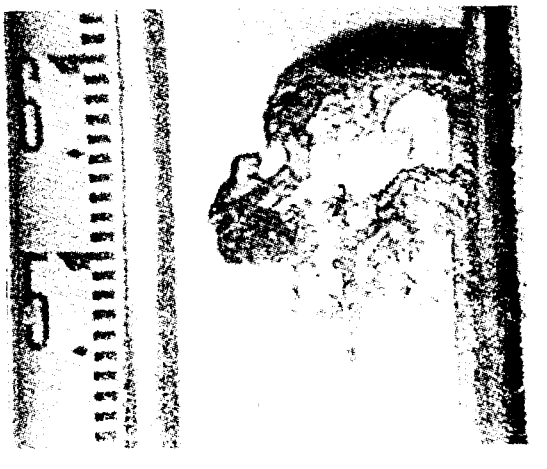

(4) 1.0 s after the cracking

Photo. 1 Rising of air bubble through water pool

NEXT PAGE(S) left BLANK